

Identification of Surface Plasmon Polariton, Hyperbolic Dispersion and Interference Regimes in Spontaneous Emission near Metamaterial Nanostructures

Kwang Jin Lee,[†] Yeon Ui Lee,[†] Yiming Xiao,^{†,‡} Loïc Mager,[§] Sang Jun Kim,^{||} Sang Youl Kim,^{||,⊥} Fabrice Mathevet,[‡] Jean-Charles Ribierre,^{†,*} Jeong Weon Wu,^{†,*} Pascal André,^{†,#*}

[†] Department of Physics, CNRS-Ewha International Research Center, Ewha Womans University, Ewha-SK Telecom Bldg. #310, Seodaemun-gu, Seoul 120-750, South Korea

[‡] Sorbonne Universités, UPMC Univ. Paris 06, CNRS, Institut Parisien de Chimie Moléculaire, UMR 8232, Chimie des Polymères, 4 Place Jussieu, 75005 Paris, France

[§] Département d'Optique Ultra-Rapide et Nanophotonique, Institut de Physique et Chimie des Matériaux de Strasbourg (IPCMS), UMR 7504, Université de Strasbourg, BP 43, 23 rue du Loess, 67034 Strasbourg Cedex 02, France

^{||} Ellipso Technology Co. Ltd., 358 Kwon Gwang-ro, Paldal-gu, Suwon 442-190, South Korea

[⊥] Department of Physics, Ajou University, 206 Worldcup Rd., Yeongtong-gu, Suwon 443-749, South Korea

[#] Elements Chemistry Laboratory, RIKEN, Wako 351-0198, Japan

Surface plasmon polariton, hyperbolic dispersion of energy and momentum, and emission interference provide opportunities to control photoluminescence properties. However, the regimes where each of them dominates or overlaps with one another remain to be clarified to fully understand and take advantage of these phenomena in optoelectronic applications. Here, we investigate, both experimentally and theoretically, broadband effects of hyperbolic metamaterial (HMM) multilayer structures on the spontaneous emission of selected organic chromophores of which emission spans across the UV-vis spectral range. The spontaneous emission lifetime of chromophores embedded in a polymer matrix located on top of HMM nanostructures is shown to vary in a non-monotonous way when the chromophore-to-surface distance is progressively adjusted. We identify surface plasmon polaritons, hyperbolic dispersion and emission interference dominant regions as a function of the emitters HMM substrate separation. We also show that the spontaneous emission lifetime is similarly affected by transverse positive and transverse negative HMMs. Finally, we provide theoretical calculations to better understand the involved mechanisms. We employ a dimensionless parameter to identify these three regimes and as a formalization tool for further studies. Calculations and experimental results are in good agreement and the former could be used to predict the photophysical responses, which could be observed when varying further the HMM nanostructures. This work has broad implications on the rational design of functional photonic surfaces to control the luminescence of organic semiconductor chromophores.

Keywords: plasmonics, hyperbolic metamaterials, emission interference, surface effects, spontaneous emission lifetime, organic semiconductors, time resolved spectroscopy

Surface and interface design nurtures very active research fields with various applications such as optical sensing,¹⁻⁴ optoelectronic devices,⁵⁻⁷ and surface-enhanced Raman spectroscopy.⁸⁻¹⁰ Controlling the structure of an environment is known to impact on photophysical properties of semiconductors. The effects can be revealed through alterations of energy and charge transfers,¹¹⁻¹³ spectral shifts and amplitude variation of both absorption and transmission,^{14,15} as well as emission amplitude.¹⁶⁻²⁰ In this context, engineering spontaneous emission rate with elaborated nanostructures is of particular interest and the effect of various structures has been explored including confinement,¹⁹⁻²² plain metal films and metal gratings,²³⁻²⁷ cavities,²⁸⁻³¹ antennas,^{32,33} photonic crystals,³⁴ nanoholes,¹⁸ metal nanoparticles,^{35,36} to name but a few.

Focusing on metal structures, important and noticeable examples of surface alterations of photophysical properties find their origins in Drexhage's early experiments. Interactions between a transient dipole and a metallic mirror have been discussed in terms of interference between the radiated field and the reflected radiation from the mirror.³⁷⁻³⁹ This leads to a non-monotonous variation of the normalized decay rate as a function of the distance from the mirror interface.^{25,40} Interference between the directly emitted field and that reflected at the metal surface results in an oscillating behavior of the spontaneous emission rate. Such an approach was recently revisited for acoustic waves,⁴¹ resonant energy transfer,¹² and charge transfer,⁴² near metal and

metamaterial interfaces. Alternatively, photonic density of state (PDOS) can be used as complementary formalism to describe luminescence decay rates near metal surfaces.²⁵ Based on Fermi's golden rule, both plasmonic coupling and interference contribute to PDOS. The effect of the former can be assessed by calculating the Purcell factor, which is strongly affected by plasmonic modes, when quantum emitters interact with plasmonic structures. In the near field, short distance range up to 20 ~ 30 nm, the emission characteristics are significantly altered due to the plasmonic coupling with the dipole radiations. In contrast, the effect of the latter takes over in the far-field through emission interference.

Beyond single metal mirrors, more complex metal structures have been explored to control the photophysical properties of semiconductors. Among them, hyperbolic metamaterials (HMMs) have drawn a lot of attention in recent years because of their unusual electromagnetic properties. HMMs are extremely anisotropic subwavelength nanostructures, which can be made of rods immersed into a dielectric environment or of stacked multilayers. In contrast with conventional dielectric media showing elliptic dispersion, HMM structures present a hyperbolic dispersion (HD), which originates from the opposite signs of the dielectric permittivity tensors of its two main components.⁴³ This results for instance in supporting high-*k* states since it was demonstrated that bulk propagating waves with large wave vectors in periodic multilayer HMMs originates from coupling of SPPs in the individual metal layers.⁴⁴ Therefore, HMMs have

been intensively studied in the context of negative refraction,^{45,46} far-field sub-wavelength imaging,⁴⁷⁻⁵¹ and spontaneous emission rate alterations.⁵²⁻⁶⁰ However, while the HMM's large PDOS was shown to increase the radiative decay rate of fluorescent emitters, it remains unclear how the transition between plamonic, HD and interference effects occurs and what parameter would be best used to formalize possible transitions from one regime to another.

In this work, we investigate these issues with a set of organic chromophores, namely 4,4''-bis[(2-butyloctyl)oxy] -1,1':4',1'':4'',1'''- quaterphenyl (BBQ), Coumarin 460 (C460) and perylene diimide (PerDi), which chemical structure is presented in Figure 1a. They were selected to be soluble in dichloromethane (DCM), to be miscible with polymethyl methacrylate (PMMA) and to span across the UV-vis spectral range. Dispersed at a low concentration in a polymethylmethacrylate solution, they were spincoated on top of four-pair HMM structures. The polymer were 35 nm thick, which is comparable to the thickness used in previous HMM studies.^{53,56} The structure of the substrates, which this work focuses on, are made of 10 nm thick Ag and Al₂O₃ alternative thin films deposited on fused silica. Focusing on the nanophotonic control of the dye emission, we tuned the thickness of the top Al₂O₃ cover, which is defined as distance d , and is schematically illustrated in Figure 1b. Seventeen different samples were prepared with the top Al₂O₃ cover thickness ranging from 10 nm to 1 μm. The effective dielectric constants $\epsilon_{x,y}$ and ϵ_z of such HMM structures can be calculated based on the effective medium approximation and display a transverse positive-to-negative transition near 375 nm as shown in Figure 1c. The optical properties of the resulting samples were then characterized experimentally by a combination of steady state and time-resolved fluorescence spectroscopies. The results were analyzed with a theoretical approach relying on

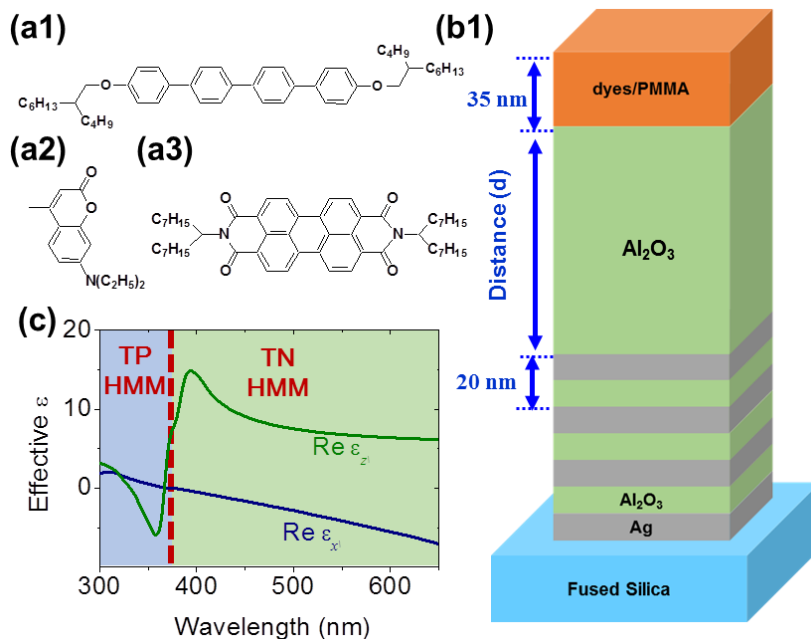


Figure 1. (a) Chemical structure of BBQ (a1), C460 (a2) and PerDi (a3). (b) Schematic of the 4-pair HMM-PMMA:dye samples. (c) Effective permittivity of the HMM used in this study. The dashed line is boundary wavelength between transverse positive (TP) HMM and transverse negative (TN) HMM.

the combination of the invariant imbedding method,^{61,62} and the finite-difference time-domain (FDTD) method.^{63,64} With these tools, we calculated the spontaneous emission rate and the Purcell factor as a function of the distance between the dye-polymer film and the top metal layer of the HMM substrates. We then identify SPPs, HD and interference emission interference dominant regions as a function of the emitters HMM substrate separation. We also show that a dimensionless parameter independent of the emission spectral range is useful to identify these three regions.

Figure 2abc1 shows the steady state normalized absorbance and

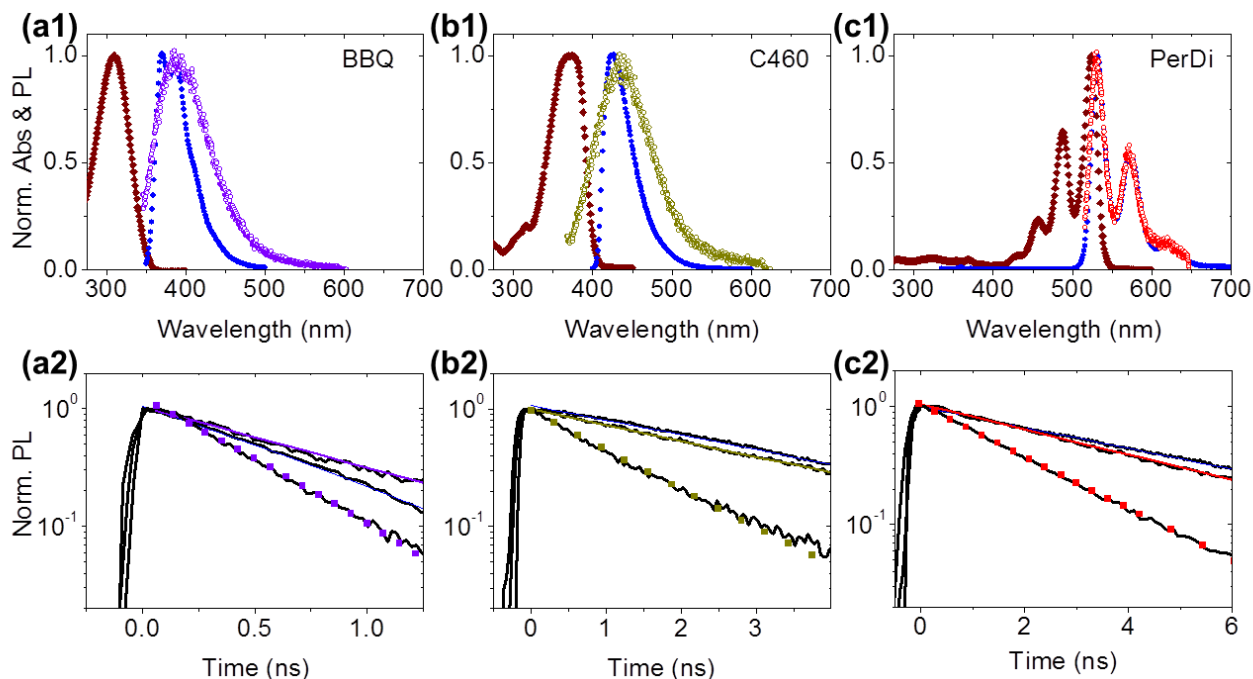


Figure 2. Photophysical properties of a selection of chromophores: (a) BBQ, (b) C460 and (c) PerDi. (1) Steady state normalized absorbance (OD, \blacklozenge) and emission (PL, \bullet) of the dyes in DCM solutions (filled symbols) and their emission in PMMA matrix from a thin film spin-coated on top of fused silica substrates (empty symbols). (2) Time resolved photoluminescence decays in DCM (thin solid line fit), in PMMA on fused silica (thick solid line fit) and in PMMA on HMM substrates (filled symbol fit, \blacksquare). The excitation wavelength of BBQ and C460 is 325 nm, while PerDi's is 470 nm.

fluorescence spectra of the three organic chromophores. The absorption and emission spectra agree well with the literature. The maximum absorbance wavelengths are 309 nm, 371 nm, and 524 nm for BBQ, C460 and PerDi, respectively. Solubilized in DCM, their photoluminescence (PL) spectra cover 350-470 nm, 405-485 nm and 520-630 nm, respectively. Immersed in a PMMA matrix, the steady state normalized fluorescence spectra of the three chromophores are slightly broader which is due to the vibronic interactions and inhomogeneous dielectric environment provided by the PMMA solid solution. A weaker effect is observed with PerDi than with BBQ and C460. The photoluminescence spectra of the three chromophores are unaffected, when spin-coated either on fused silica (FS) or on HMM substrates (see Figure S1).

Streak camera measurements were performed to monitor the evolution of the spontaneous emission lifetimes for BBQ, C460 and PerDi. The resulting streak images of three chromophores in PMMA on FS and HMM are shown in Figure S2 to S4. Integrations of the streak camera signal along the time axis within the emission spectral regions are shown in Figure 2abc2. All the time resolved PL spectra, regardless of the solvent, matrix and substrate conditions, display a mono-exponential decay, indicating that there is no significant aggregation in either solution or film. The PL lifetime values are summarized in Table S1. Within 10 %, the emission dynamics of three chromophores are identical when measured in DCM and in PMMA on FS. As expected from the literature, dyes in PMMA spincoated on HMM structures present a noticeably faster PL decay. Decay time of each sample in the presence of HMM significantly decreases over the whole spectral range herein considered. This acceleration of the spontaneous emission on HMMs is then confirmed to be a broadband effect.

Theoretical calculations of the normalized spontaneous emission lifetimes at three wavelengths relevant to BBQ, C460 and PerDi ($\lambda_{\text{PL}} = 365 \text{ nm}$, 450 nm and 535 nm) are shown in Figure 3a. The calculations were performed using the following equations:²⁵

$$\tau_{\parallel}(\zeta) = \tau_0 \left[1 + \frac{3}{4} q \operatorname{Im} \left(\int_0^{\infty} [(1-u^2)r_p + r_s] e^{-2w\zeta} \frac{u}{w} du \right) \right]^{-1} \quad (1)$$

$$\tau_{\perp}(\zeta) = \tau_0 \left[1 - \frac{3}{2} q \operatorname{Im} \left(\int_0^{\infty} r_p e^{-2w\zeta} \frac{u^3}{w} du \right) \right]^{-1} \quad (2)$$

where τ_{\parallel} and τ_{\perp} are the decay times of radiative dipoles having parallel and perpendicular orientations, respectively, when compared with the multilayered HMM structures. For sake of simplicity, we define $\zeta = d \cdot k_d$ as the dimensionless parameter characterizing the minimum distance of the transient dipoles from the last HMM Ag layer (i.e. spacer thickness) in terms of wavevectors. τ_0 is the intrinsic PL lifetime of the emitter. q is the radiative quantum efficiency of the emitter, $u = (k_d)_x/k_d$ is the wavevector ratio, and with $w = -i(1-u^2)^{1/2}$. $(k_d)_x$ and k_d are the wavevectors inside the Al_2O_3 spacer layer, respectively. They are given by $2\pi n_d/\lambda_{\text{PL}}$ where n_d is the refractive index of spacer layer and λ_{PL} the emission wavelength of the radiative dipole. Finally, r_s and r_p are the reflection coefficients for s - and p - polarized

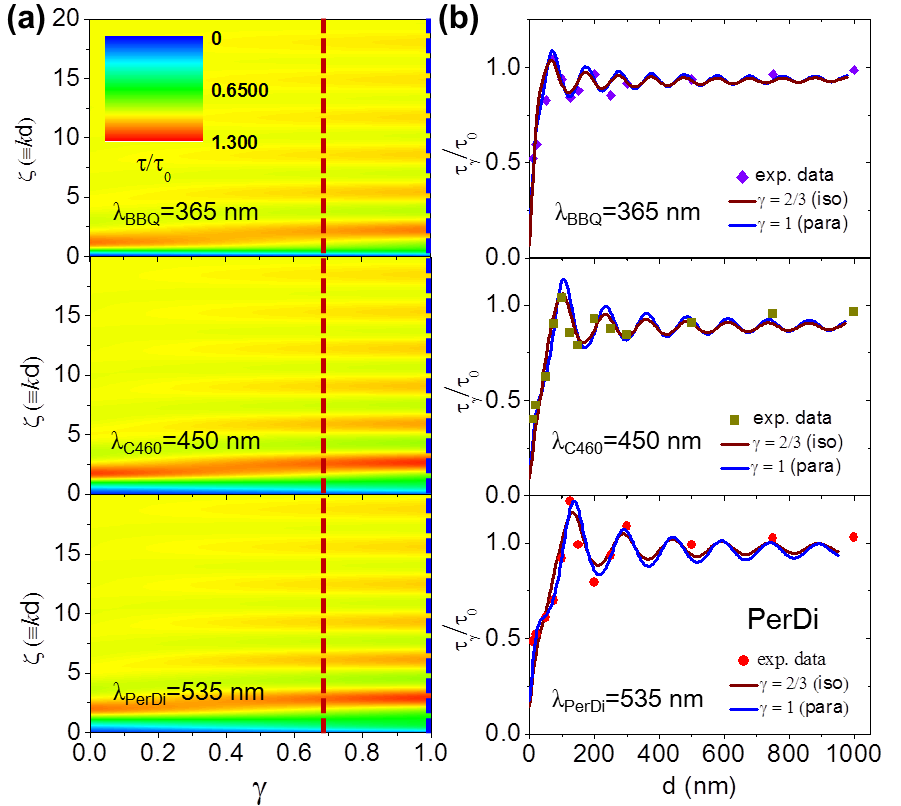


Figure 3. Effect of HMM spacer on spontaneous emission lifetime. (a) Pseudocolor plot of the calculated spontaneous emission lifetime as a function of the dimensionless distance ($\zeta = 2\pi d n_d/\lambda_{\text{PL}}$) and the dipole orientation (γ) for three wavelengths (365 nm, 450 nm, 535 nm) characteristic of the emission of the BBQ, C460 and PerDi emitters, respectively. The vertical dashed lines materializes isotropic (red) and parallel (blue) orientations of the emitting dipoles (b) Normalized spontaneous emission lifetimes for three emitters as a function of distance : experimental data (symbol), theoretical calculations (lines) where brown and blue lines correspond to $\gamma = 2/3$ and $\gamma = 1$, respectively.

electromagnetic waves, respectively. As detailed in the SI, in order to obtain the exact values of r_s and r_p of the HMM structures, we employed the invariant imbedding method for the electromagnetic wave propagation in the HMM structures. The equations of the reflection coefficients r_s and r_p are obtained and integrated for each thickness of the HMM top dielectric layer.^{60-62,65} With this approach, any dipole orientation, defined as γ , is considered as a linear combination of parallel and perpendicular dipole components. The decay time for any orientation is

$$\tau_{\gamma} = \gamma \tau_{\parallel} + (1-\gamma) \tau_{\perp} \quad (3)$$

Figure 3a shows the normalized spontaneous emission decay times τ/τ_0 , i.e. the ratio of the spontaneous emission decay time of chromophores located on top of HMM and on top of fused silica substrates, as a function of both ζ (vertical axis) and γ (horizontal axis), where blue and red represent slower and faster relative radiative lifetime, respectively. The three wavelengths, $\lambda = 365$, 450 and 535 nm , correspond to the emission maximum of of BBQ, C460 and PerDi, respectively. The overall behavior of τ/τ_0 is the same for the three chromophores under consideration: near the substrate, small ζ value, a shorter emission lifetime occurs, it then rises to a maximum value larger than one, and eventually displays periodic and damped oscillations with ζ . $\tau/\tau_0 = 1$ is eventually reached far from the HMM structure. With an orientation of the dipole perpendicular to the substrate, the damping takes place very close to the HMM structure. However, when the radiative dipoles become parallel to the substrate the amplitudes of the τ/τ_0 oscillation are larger and remain noticeable far from the HMM structure. We note that, with the emission wavelength of the transient dipole, the maximum value of τ/τ_0 increases and the green zone near the HMM structure appears to stretch over a wider ζ range.

Figure 3b presents cross-sections of Figure 2a for dipoles with isotropic and parallel orientation ($\gamma = 2/3$ and 1) as a function of dimensionless distance, ζ , and confirms the main features described in Figure 2(b). Furthermore, Figure 2b shows a good agreement of the calculated and experimental data obtained with BBQ, C460 and PerDi. The positions of the first τ/τ_0 maximum of three chromophores are 75, 100 and 125 nm, respectively. The τ/τ_0 periodicities are 105 nm, 133 nm and 155 nm, which is directly related with the emission wavelength of the radiative dipole and corresponds to $\lambda/(2n_d)$, as illustrated in SI. Two differences between the three chromophores are nonetheless noticeable. First, BBQ and PerDi experimental results are more consistent with the calculations completed for $\gamma = 1$ rather than $\gamma = 2/3$. In contrast, the C460 experimental data are more consistent with the $\gamma = 2/3$ calculations. As further illustrated in Figure S5, this suggests that the chromophore orientations differ slightly in the PMMA matrix. This might result from the size and shape of the molecules, the smaller the more isotropic the orientation. This is consistent with works showing a horizontal orientation of light-emitting chromophores in spin-coated guest-host systems.^{66,67} In addition, we note that for short distances from the HMM structure, τ/τ_0 presents a kink before reaching its maximum values. As displayed in Figure S6, positive and negative kinks are observed for BBQ and PerDi, respectively. These two chromophores also present the shortest and longest emission wavelength. To focus on this aspect, PerDi was selected for experimental convenience, because this chromophore is associated with the largest τ/τ_0 value, which is located the furthest away from the HMM structure allowing an easier modulation of the dielectric spacer thickness.

Figure 4 displays experimental data and calculations of τ/τ_0 as a function of distance from substrates composed of a different number of Ag/Al₂O₃ pairs with dipoles emitting at $\lambda = 535$ nm. It is made with cross-sections of the pseudocolor plots shown in Figure S7 of the emission lifetime ratio calculated as a function of

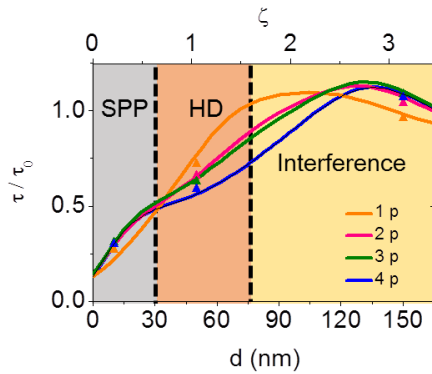


Figure 4. Emission lifetime ratio of transient dipoles at 535 nm: Calculations (solid line) and experimental data of PerDi (symbols) of normalized fluorescence lifetime as a function of distance from HMM structure composed of 1 to 4 Ag/Al₂O₃ pairs and as a function of the dimensionless parameter ζ .

Table 1. Experimental values of τ/τ_0 ratio for PerDi at 10 nm, 50 nm and 150 nm distances from the substrates composed of 1 to 4 Ag/Al₂O₃ pairs.

	10 nm	50 nm	150 nm
1 p	0.27 ± 0.04	0.72 ± 0.02	0.96 ± 0.02
2 p	0.30 ± 0.03	0.66 ± 0.02	1.04 ± 0.01
3 p	0.31 ± 0.03	0.63 ± 0.02	1.09 ± 0.01
4 p	0.30 ± 0.03	0.59 ± 0.02	1.07 ± 0.01

distance and orientation parameter for 1~4 Ag/Al₂O₃ pairs. As summarized in Table 1, near the HMM structures, experimental errors do not allow to discriminate between τ/τ_0 measured on different number of pairs. Further away, τ/τ_0 values appear to decrease when increasing p , whereas the opposite behavior is observed even further. Noticeably, these experimental data are in good agreement with the calculated τ/τ_0 extracted from the full calculations provided in Figure S7. These cross-sections shed new light on the experimental data. For any number of pairs the variation of τ/τ_0 with d is non-monotonous. Overall, τ/τ_0 increases up to a maximum larger than one and decreases. This is consistent with the behavior of 4 p HMM structures reported in Figure 2. Interestingly, the distance, at which this maximum occurs, is only shorter for 1 p but barely varies for $p > 2$. The first maximum distance of τ/τ_0 and maximum value of τ/τ_0 with p are plotted in Figure S8. The inversion of τ/τ_0 with the number of pair is associated with the transient dipole being closer or further away than the position at which the maximum value of τ/τ_0 occurs. Furthermore, the kink previously mentioned is not visible at $p = 1$, but it appears and strengthens with p . These observations suggest that beyond the generality of the present observation as evidenced both experimentally and numerically, several phenomena take place near the HMM interface, each of them being important within a particular range of distances between the chromophore and the HMM.

For very small distances ($d \leq 30$ nm), corresponding to the evanescent near field, transient dipoles excite propagating surface plasmon polaritons (SPP) in the metal layers located nearby. A partial transfer of energy into heat also occurs due to losses in metal. Through these processes, the photonic density of states (PDOS) increases and the non-radiative decay rate increases,^{65,68} as a result, the photoluminescence lifetime is strongly reduced.⁵⁴ This is consistent with the experimental τ/τ_0 data obtained on top of a 10 nm Al₂O₃ spacer, which do not show any measurable difference with the number of pairs. Importantly, we note that the reduction of PL lifetime is mostly affected by the top metallic layer, which means that the HD of four-pair multilayer is not responsible in the regime of $d \leq 30$ nm. The slight difference in τ/τ_0 between 1 pair and 2~4 pairs shown in Figure 4 is associated with the very high Purcell factor around 550 nm for 1 pair substrate as shown in Figure S9. Putting aside this high Purcell factor of the 1 p structure which occurs coincidentally in the same spectral range as the emission of the PerDi, the fact that transient dipoles cannot be affected by HD for very small d is consistent with HMMs being defined as a result of effective medium theory. Within the intermediate range of distances ($30 \text{ nm} \leq d \leq 75 \text{ nm} = \lambda/4n_d$), the PDOS is altered by the HD, leading to the increase of the radiative relaxation channels. The PL decay characteristic time shortens with the number of Ag/Al₂O₃ pairs as shown in table 1 ($d = 50$ nm). This behavior is consistent with the fact that radiative channels are known to increase when the emitter is located nearby HMMs.⁵⁴ Furthermore, we note that when $d < \lambda/4n_d$, non-radiative energy transfer from the excited molecules to the metal could also occur through dipole-dipole interaction.²⁵ For distances longer than $d = \lambda_{\text{PL}}/4n_d \geq 75$ nm, an oscillating variation of τ/τ_0 with a $\lambda_{\text{PL}}/2n_d$ periodicity is imposed by an interference effect resulting from the superposition of the emitted light field and its reflection at the HMM interface. This leads to a PL lifetime behavior opposite to that taking place in the intermediate regime as the number of pairs of multilayer increases. As shown in table 1 for $d = 150$ nm, τ/τ_0 increases with the number of pairs, while τ/τ_0 decreases with the number of pairs for $d = 50$ nm. Even if a contribution of the HD cannot be ruled out, its relative impact on the photoluminescence dynamics appears to be small compared to the interference effect contribution. The resulting oscillating behavior of τ/τ_0 as a function of distance can be described in terms of interference induced PDOS changes. In Figure S10, calculations of τ/τ_0 as a

function of distance at three wavelengths are plotted. At 365 nm, τ/τ_0 get reduced with increasing the number of pairs for $d = \lambda_{PL}/4n_d \leq 50$ nm. It is hard to find the SPP dominated regime since 365 nm is out of the surface plasmon resonance of Ag with Al_2O_3 .

To summarize our findings, in the present studies three distinct dyes covering a wide spectral range were used to identify the general behavior of transient dipoles near HMM and to evidence the overlap of several phenomena. The chromophore with the lowest transition energy and HMM substrates with different number of pairs were then used to identify these phenomena and 3 regimes in which SPP, HD and interference effects were dominant. The final part of this work is interested in the effect of the boundary between transverse positive (TP, where $\epsilon_{x,y} > 0$ and $\epsilon_z < 0$) and transverse negative (TN, where $\epsilon_{x,y} < 0$ and $\epsilon_z > 0$) of the Ag: Al_2O_3 HMM structures. For this reason, we now focus on the SPP, HD regimes and consider three chromophores and compare results obtained through optical and FDTD numerical calculations.

As illustrated in Figure 4a, the emission spectrum of BBQ lies across the TP and TN HMM spectral regimes, while those of C460 and PerDi lie in the TN HMM region only. Calculation and experimental results of inverse of τ/τ_0 , as a function of the dimensionless parameter and the distance are shown in Figure 4b and 4c, respectively. It is noticeable that experimental data and theoretical calculations based only on the optical properties of the substrate show similar trends in both representations. Across both the SPP and HD regimes, a qualitative agreement is then observed with longer (smaller) decay time (rate) for BBQ at 365 nm than for C460 at 450 nm and PerDi at 535 nm. This was confirmed with a fourth chromophore (2,5-diphenyloxazole) whose emission spectral range is slightly lower than BBQ's as shown in Figure S12. A qualitative agreement is observed between the experimental data and the optical reflection numerical approach, with for instance of the relative PL lifetime

being systematically slower for emissions near the TP to TN boundary wavelength. This is attributed to the different PDOS in the TP and TN HMM regimes.

In order to support this hypothesis, the Purcell factor (PF) was calculated by the FDTD method as a function of the distance from Ag/ Al_2O_3 4-pair HMMs over the whole spectral region considered in this study. Figure 4d shows that the Purcell factor strongly depends on the distance and wavelength; maxima are located near the HMM interface and at any incident wavelength PF decreases with distance.

More accurate reading can be obtained with cross-sections as illustrated in Figure 4e. Two peaks are then clearly visible. The first around 360 nm corresponds to silver plasmon resonance. The second at longer wavelength corresponds to coupling between the metal layers as illustrated by the cross-sections of the Purcell factor taken at $d = 10, 20, 30, 50, 90$ nm (black dashed lines) from Figure 4d. Overall, the Purcell factor in TP HMM regime is lower than that in TN HMM regime. The peak and shoulder shown at $d = 10$ nm and 20 nm, respectively, are associated with the surface plasmon resonance of Ag film. Since the Purcell factor is proportional to local density of state,^{69,70} Figure 4e is consistent with a previous numerical study showing that local density of state in TP HMM regime is lower than that in TN HMM regime.⁷⁰

We also plotted the cross-sections of the Purcell factor taken at $\lambda_{PL} = 365, 450$ and 535 nm (white dashed lines) from figure 4d and experimental data of normalized decay rate for three chromophores. The results shown in Figure 4f clearly demonstrate that the Purcell factor and emission decay rate enhancement of organic chromophores in TP HMM regime are smaller than those in TN HMM regime up to $d = \lambda/4n_d$, which correspond to the region in which interference effects start to dominate the spontaneous emission.

Figure S13, corresponds to the Purcell factor calculations obtained for a single 70 nm thick Ag film substrate. Comparing Figure 4 and Figure S13 shows that the Purcell factor in the

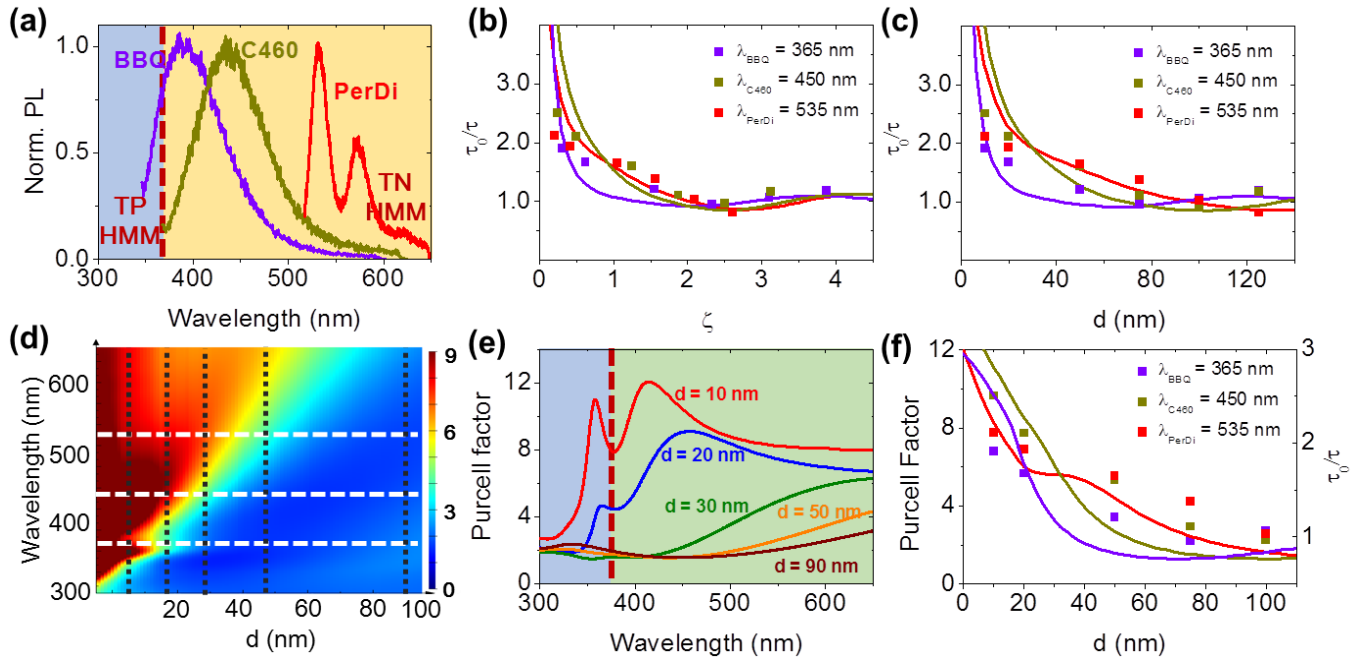


Figure 4 (a) Fluorescence spectra of three chromophores dispersed in PMMA matrices; the vertical dashed line is the boundary wavelength between transverse positive (TP) and transverse negative (TN) of 10nm:10nm Ag: Al_2O_3 HMM structures. (b, c) Analytical calculations and experimental data of normalized spontaneous emission rates for $\lambda_{PL} = 365, 450$ and 535 nm for three chromophores as a function of the dimensionless parameter (b) and distance (c). (d) Pseudocolor plot of Purcell factor as a function of wavelength and distance from 4 Ag/ Al_2O_3 pair HMMs. (e) Cross-sections of the Purcell factor as a function of wavelength taken at $d = 10, 20, 30, 50$ and 90 nm. (black dash line) (f) Purcell factor (solid line) as a function of distance for three wavelengths (365, 450, 535 nm, white dash line) and the inversed of normalized experimental decay rate τ_0/τ (symbol) for the chromophores as a function of distance.

presence of HMM presents a broadband frequency tunability as a function of distance d and this demonstrates that broadband Purcell peak results from the higher number of hybridized plasmonic modes made available to the emitter. This are shown in Figure S14.

In this letter, we have provided two theoretical descriptions based on two different methods, analytical formalism combined with invariant imbedding method and Purcell factor using FDTD simulations, to support our experimental results. Overall trends of experimental results and two calculations are consistent with one another, while the differences between two theoretical results come from parameters such as the reflection coefficients obtained by the invariant imbedding method, mesh step size in FDTD simulations (see Method in SI).

In conclusion, the overall characterization of spontaneous emission properties of a range of organic emitters near HMM structures was completed by changing the number of metal-dielectric pairs as well as spacing between emitters and HMMs.

Interestingly we identified three distinct regimes. First, we evidenced an emission-interference dominant regime near HMMs similar to behaviors observed in the literature near single metal layers. Next, we confirmed that very close to HMMs, SPPs dominate PL lifetime behaviors and lead to a decrease of spontaneous emission lifetime regardless of the number of metal-dielectric pairs. In addition and more importantly, we found the existence of a third regime where HD dominates and leads to a non-monotonous variation of the spontaneous emission lifetime of organic chromophores. The resulting kink has an on-set at the boundary between SPP and HD regimes. To the best of our knowledge, this is the first report demonstrating that such a specific feature is characteristic of a HD dominant regime.

We also confirmed that enhancement of emission decay rate of BBQ (and PPO) is smaller than C460 and PerDi cases due to the fact that Purcell factor is relatively high in TN HMM regime compared to TP HMM regime. Experimental realizations of these effects have not been reported before. The results also suggest that the dimensionless parameter $\zeta = d \cdot k_d$ could be taken advantage of to further explore and describe these regime transitions.

This work sheds new lights on semiconductor photoluminescence properties near metamaterial substrates. It will assist their use to control the spontaneous emission of molecules for fundamental and applied investigations. Based on the present fundamental study, further improvements can be realized by rationally designing and optimizing HMM structures to provide desired tunability of Purcell factor enhancement with high emission rate across broadband spectral regions.

Methods

Chemicals: 4,4''-bis[(2-butyloctyl)oxy] -1,1':4,1''-4,1''- quaterphenyl (BBQ), Coumarin 460 (C460), and 2,5-Diphenyloxazole (PPO) were purchased from Exciton. perylene diimide (PerDi) was synthesized according the literature. Polymethyl methacrylate (PMMA, Mw = 50 kD) and dichloromethane (DCM) were purchased from Sigma-Aldrich.

Steady-state absorbance and fluorescence measurements: UV-vis absorption spectra were recorded on a Hitachi U-3310 spectrophotometer. Steady-state fluorescence spectra were obtained using a Varian Cary Eclipse spectrofluorimeter.

Time-resolved photoluminescence measurements were carried out using the streak camera (Hamamatsu) with a time resolution of about 10 ps. The pulse duration was 60 fs and the repetition rate was 5 kHz. The excitation wavelengths used for our experiment was either 325 nm or 470 nm. The emission light was collected at the magic angle between the polarization of the excitation light and the polarization of the detected polarized light in order to avoid any polarization anisotropy effects. The photoluminescence decays were fitted by a single exponential model.

Spectroscopic ellipsometry was completed with the SE ellipsometer from Ellipso technology Co., Inc., used in the measurement of the rotating polarizer type.

The analytical and numerical calculation methods are described in the SI.

References

- (1) Kabashin, A. V., et al. Nature materials **2009**, 8, 867-871.
- (2) Heller, D. A., et al. Nat. Nanotechnol. **2009**, 4, 114-120.
- (3) Hao, F., et al. ACS Nano **2009**, 3, 643-652.
- (4) Vautravers, N. R., et al. J. Mater. Chem **2009**, 19, 4545.
- (5) Kim, R. H., et al. Nat. Comm. **2014**, 5, 3583-3595.
- (6) Howells, C. T., et al. J. Mater. Chem. A **2016**, 4, 4252-4263.
- (7) Ribierre, J. C., et al. Chem. Comm. **2015**, 51, 5836-5839.
- (8) Camp Jr, C. H.; Cicerone, M. T. Nat. Photonics **2015**, 9, 295-305.
- (9) Wen, X. L., et al. Nanoscale **2014**, 6, 132-139.
- (10) Zhang, R., et al. Nature **2013**, 498, 82-86.
- (11) Andrew, P.; Barnes, W. L. Science **2004**, 306, 1002-1005.
- (12) Blum, C., et al. Phys. Rev. Lett. **2012**, 109, 203601.
- (13) Lee, K. J., et al. Under revision **2016**, <http://arxiv.org/abs/1510.08574>.
- (14) Ebbesen, T. W., et al. Nature **1998**, 391, 667-669.
- (15) Hutchison, J. A., et al. Angewandte Chemie **2011**, 50, 2085-2089.
- (16) Lakowicz, J. R., *Principles of Fluorescence Spectroscopy*. Springer-Verlag US: 2006;
- (17) Fort, E.; Grésillon, S. J. Phys. D **2008**, 41, 013001.
- (18) Wenger, J., et al. Opt. Express **2008**, 16, 3008-3020.
- (19) André, P., et al. J. Phys. Chem. B **2008**, 112, 16382-16392.
- (20) Ribierre, J. C., et al. Phys. Chem. Chem. Phys. **2016**, 18, 3575-3580.
- (21) Larson, D. R., et al. Chem. Mater. **2008**, 20, 2677-2684.
- (22) Chen, S., et al. Chem. Comm. **2012**, 48, 2501-2503.
- (23) Worthing, P. T., et al. Phys. Rev. A **1999**, 59, 865-872.
- (24) Amos, R. M.; Barnes, W. L. Phys. Rev. B **1999**, 59, 7708-7714.
- (25) Barnes, W. L. J. Mod. Opt. **1998**, 45, 661-699.
- (26) Andrew, P.; Barnes, W. Phys. Rev. B **2001**, 64.
- (27) Astilean, S., et al. J. Mol. Struct. **2003**, 651, 277-283.
- (28) Cho, C. H., et al. Nat. Mater. **2011**, 10, 669-675.
- (29) Russell, K. J., et al. Nat. Photonics **2012**, 6, 459-462.
- (30) Kroekenstoel, E. J. A., et al. Appl. Phys. Lett. **2009**, 95, Artn 263106.
- (31) Ballarini, D., et al. Adv. Opt. Mater. **2014**, 2, 1076-1081.
- (32) Belacel, C., et al. Nano Lett. **2013**, 13, 1516-1521.
- (33) Rogobete, L., et al. Opt. Lett. **2007**, 32, 1623.
- (34) Lopez-Garcia, M., et al. Small **2010**, 6, 1757-1761.
- (35) Ming, T., et al. Nano Lett. **2009**, 9, 3896-3903.
- (36) Darby, B. L., et al. Nat. Photonics **2016**, 10, 40-U54.
- (37) Drexhage, K. H. J. Lumin. **1970**, 1-2, 693-701.
- (38) Drexhage, K. H., et al. Ber. Bunsen Ges. Phys. **1968**, 72, 329.
- (39) Drexhage, K. H. Sci. Am. **1970**, 222, 108-119.
- (40) Chance, R. R., et al., Molecular Fluorescence and Energy Transfer Near Interfaces. In *Advances in Chemical Physics*, Prigogine, I.; Rice, S. A., Eds. 1978; Vol. 37, pp 1-65.
- (41) Langguth, L., et al. Phys. Rev. Lett. **2016**, 116, 224301.
- (42) Lee, K. J., et al. In preparation **2016**.
- (43) Poddubny, A., et al. Nat. Photonics **2013**, 7, 948-957.
- (44) Zhukovsky, S. V., et al. Opt. Express **2013**, 21, 14982-14987.
- (45) Argyropoulos, C., et al. Opt. Express **2013**, 21, 15037-15047.
- (46) Sreekanth, K. V., et al. Appl. Phys. Lett. **2013**, 103, 023107.
- (47) Liu, Z., et al. Science **2007**, 315, 1686.
- (48) Lu, D.; Liu, Z. Nat. Commun. **2012**, 3, 1205.
- (49) Jacob, Z., et al. Opt. Express **2006**, 14, 8247.
- (50) Wei, F.; Liu, Z. Nano Lett. **2010**, 10, 2531-2536.
- (51) Bak, A. O., et al. Nano Lett. **2016**, 16, 1609-1613.
- (52) Kidwai, O., et al. Opt. Lett. **2011**, 36, 2530-2532.
- (53) Noginov, M. A., et al. Opt. Lett. **2010**, 35, 1863-1865.
- (54) Kim, J., et al. Opt. Express **2012**, 20, 8100-8116.
- (55) Lu, D., et al. Nat. Nanotech. **2014**, 9, 48-53.
- (56) Shi, J., et al. Nano Lett. **2015**, 15, 1217-1221.
- (57) Tumkur, T., et al. Appl. Phys. Lett. **2011**, 99, 151115.
- (58) Jacob, Z., et al. Appl. Phys. B **2010**, 100, 215-218.
- (59) Poddubny, A. N., et al. Phys. Rev. A **2011**, 84.
- (60) Noginov, M. A., et al. Appl. Phys. Lett. **2009**, 94, 151105.
- (61) Lee, K. J., et al. Opt. Express **2013**, 21, 28817-28823.
- (62) Lee, K. J., et al. pt. Mater. Express **2014**, 4, 2542.
- (63) Lee, Y. U., et al. Opt. Express **2014**, 22, 20816-20827.
- (64) <https://www.lumerical.com/>
- (65) Kim, K., et al. J. Korean Phys. Soc. **2001**, 39, L956-L960.

- (66) Zhao, L., et al. Appl. Phys. Lett. **2015**, 106, 063301.
(67) Zhao, L., et al. submitted **2016**.
(68) Pockrand, I., et al. Chem. Phys. Lett. **1980**, 69, 499-504.
(69) Novotny, L.; Hecht, B., *Principles of nano-optics*. 2nd ed. ed.; Cambridge University Press: Cambridge, 2012;
(70) Cortes, C. L., et al. J. Opt. **2012**, 14, 063001.

Acknowledgments

This work has been carried out in the framework of the CNRS International Associated Laboratory "Functional nanostructures: morphology, nanoelectronics and ultrafast optics" (LIA NANOFUNC). KJL, YUL, YX, JCR, JWW and PA were supported by funding of the Ministry of Science, ICT & Future Planning, Korea (201000453, 2015001948, 2014M3A6B3063706). PA would like to thank the Canon Foundation in Europe for supporting his Fellowship. YX and FM acknowledge the International Research Network (GDRI, CNRS) on "Functional Materials for Organic Optics, Electronics and Devices" (FUNMOOD).

Author Contributions

KJL, JCR, JWW and PA discussed the principles of the study. KJL, JWW and PA conceived and designed the experiments. YX synthesized the perylene diimide under FM supervision. KJL prepared the samples and completed both the time resolved measurements and their analysis with the feedback of PA. LM and JCR contributed to the first dye measurements and commented on its concentration, respectively. KJL, SJK and SYK completed and analyzed the ellipsometry measurements, which were discussed with PA and JWW. KJL and YUL completed the invariant embedding method calculations and FDTD calculations, respectively. KJL and PA organized the results and KJL prepared the figures. KJL and PA organized the results and KJL prepared the figures. KJL wrote the manuscript and SI with feedbacks from PA and JWW. All the authors could comment the manuscript.

Additional Information

Supplementary information is available in the on-line version of the paper:

Notes

The authors declare no competing financial interest.